International Journal of Automotive Technology, Vol. 1, No. 2, pp. 79–87 (2000)

1229–9138/2000/002–03

THERMO-MECHANICAL ANALYSIS OF OPTICALLY ACCESSIBLE QUARTZ CYLINDER UNDER FIRED ENGINE OPERATION

K. S. LEE* and D. N. ASSANIS

Department of Mechanical Engineering, University of Michigan, Ann Arbor, MI 48105-2121, U.S.A.

(Received 30 August 2000)

ABSTRACT–Analytical approach was followed in this work under both the steady state and transient operating conditions to find optimum boundary conditions, where the optically accessible quartz engine can run safely without breaking. Temperature and stress distribution was predicted by FEM analysis. In order to validate thermal boundary condition, model reliability and constraint, outside cylinder temperature was measured and previous study was also followed up numerically. To reduce thermal stress level, three types of outside cooling (natural, moderate forced and intensive forced convection) were considered. Effects of clamping force and combustion pressure were conducted to investigate mechanical stress level. Cylinder thickness was changed to find the optimum cylinder thickness. The versatile results achieved from this work can be basic indication, which is capable of causing a sudden quartz cylinder breaking during fired operation.

KEY WORDS : Quartz engine, FEM, Thermal stress, Mechanical stress, Forced convection

1. INTRODUCTION

Engine visualization is a necessary first-step to obtain an overall understanding of in-cylinder events. Visualization combined with knowledge of basic principles can provide new insights into the operation of the system and may suggest changes to be made that could improve performance. The major difficulty in visualization in engine cylinder is having useful access to the cylinder interior while the engine is running. In addition, the cylinder in most engines is surrounded by complex structures that are an obstacle for even limited optical access. The results have been developed some unusual engines and pseudo-engines.

To visualize inside engine cylinder without any interference, the engine cylinder material has to be transparent, strong, able to withstand high temperature, resistant to thermal stress, and reasonably hard. Fused quartz and single crystal sapphire have been considered seriously as cylinder materials in order to visualize in-cylinder gas motion because of their special material properties.

Pure sapphire is colorless and has an appearance similar to good quality optical glass. However, the disadvantages of sapphire are brittle, a high coefficient of thermal expansion and very expensive. The high coefficient of thermal expansion means that thermal gradient can induce significant stresses. The brittleness of sapphire also makes it susceptible to stress concentration caused by point contacts in a poorly designed mount. Sapphire is the third hardest material known with a MOH rating of 9.

It is difficult to polish but able to withstand rubbing of materials. Unfortunately, in practice, it is fairly easy to scratch and particles can be trapped in a rubbing surface. And the cost of pure sapphire is a big issue because the sapphire cylinder has lots of possibility of frequent breaking during engine operation. An alternative material for engine visualization is quartz. Quartz is the optical material most commonly used both for commercial purpose and for research. Its design fracture strength in tension is much smaller than sapphire. Although quartz has a much lower coefficient of thermal expansion than sapphire, it is also subject to large thermal stresses relative to its strength. The primary difficultly with using quartz is that it is fragile when handled.

A consistently high level of care is necessary in an engine application, since the liner must be removed and cleaned many times. And high level mounting techniques are also needed at structural contact points. Another problem is scratching of the inner surface due to particles embedded in the rings, as with sapphire. Nevertheless, the reason for alternative using of quartz is cheaper and

*Corresponding author. e-mail: kslee@ytbi.co.kr

Table 1. Typical properties of sapphire and quartz.

Property	Ultimate tensile strength ($Pa \times 10^6$)	Young's modulus ($Pa \times 10^9$)	Poisson's ratio	Thermal expansion coefficient ($°C^{-1} \times 10^{-6}$)	Thermal conductivity (W/m°C)	Density ($Kg/m^3 \times 10^3$)	Thermal diffusivity ($m^2/sec \times 10^{-6}$)	Melting point (°C)
Sapphire	400	390	0.15	8	25	4.0	7.2	2040
Quartz	50	70	0.16	0.6	1.4	2.2	0.8	1700

better optical properties than sapphire. Typical material properties of sapphire and quartz are compared in Table 1.

1.1. Review of Optical Access in Engine with Quartz

The effort to visualize engine cylinder phenomena began with a glass cylinder by Otto in 1872. An operating engine with a quartz piston was developed by Bowditch (Bowditch, 1961). In that study, the original piston was replaced by an elongated hollow piston with a fused quartz window mounted in its face. Withrow and Rassweiler and later Nakanishi *et al.* were used quartz window mounted L-head engines and photographed combustion phenomena (Withrow, 1936; Nakanishi, 1975). Oppenheim et al. developed square fused quartz sidewall in engine cylinder to photograph combustion events (Oppenheim, 1976). The same apparatus was used by Ishikawa and Daily to study details of the flow with a conventional single-pass schlieren system (Ishikawa, 1978). Holtman and McClure visualized diesel engine flows by a single cylinder with a thick (2.2 mm), fused quartz cylinder and operated this engine under motored and limited fired condition – limited number of cycle (Holtman, 1978). An engine with transparent sidewalls made of fused quartz was built by Namazian *et al.* (Namazian, 1980). A single cylinder research engine made of a 1.72 mm thick quartz liner for flow visualization was built by Bates (Bates, 1988) and was used for motoring studies. They reported that one quartz liner survived for 11 months of intermittent operation while accumulating some large chips on the top outside from mounting errors, and some small chips on the bottom inside from assembly errors. And it finally failed due to thermal stresses during a 25 minute motoring test at low speed with graphite rings. In previous works reviewed, the optical engine design was a compromise between the optical accesses required and engine components.

Experience in our laboratory suggests five major cause of cylinder failure including (1) thermal stresses, (2) maximum pressure loads, (3) clamping loads, (4) local stresses due to chipping, and (5) thermal expansion of rings. The purpose of this study was to conduct thermal and stress analysis with two goals in mind; (1) what is the best design and operation procedure to minimize failure due to thermal stresses and (2) is it possible to identify a measurable precursor that can predict failure? In pursuit of the fore mentioned two goals, a three dimensional thermal and stress analysis is performed that includes modeling of three dimensional thermal boundary conditions, cylinder pressure, clamping loads, frictional heating, and convection (free and forced).

2. FEM ANALYSIS

A three dimensional finite element model of the cylinder was composed and a total of 8,320 nodes and 700 elements were employed to describe the FEM model using cartesian coordinate. 1-D or 2-D modeling can save computational costs and efforts. However, the target engine has two quartz windows on the top and for better understanding of 3-D temperature and stress field, 3-D modeling was required. Steady state and transient heat transfer and stress analysis was accomplished using the commercial codes Hypermesh 3.0 (pre- and post-processor) and ABAQUS 5.8 (solver). The heat transfer analysis was conducted first. Subsequently, the heat transfer results and combustion pressure were used to perform the stress analysis. Figure 1 shows schematic diagram of imposed boundary conditions.

2.1. Basic Assumptions

During the real engine operation, engines are under time varying coupled thermal (due to heat input from combustion and piston ring friction) and mechanical load (due to clamping forces and combustion pressure). To describe realistic engine operating conditions by FEM analysis, several reasonable assumptions are needed. In this study, engine operation was assumed to be quasi steady state at given time step and cyclic thermal shock effect in thermal penetration depth was ignored. Combustion pressure and heat fluxes were assumed to be constant profiles in time, but decreased along the liner longitudinal direction from the liner top. Effect of quartz window was assumed to be adiabatic condition and clamping force was assumed to be evenly distributed pressure on liner top and bottom. Frictional heat source was assumed to be stepwise function and friction

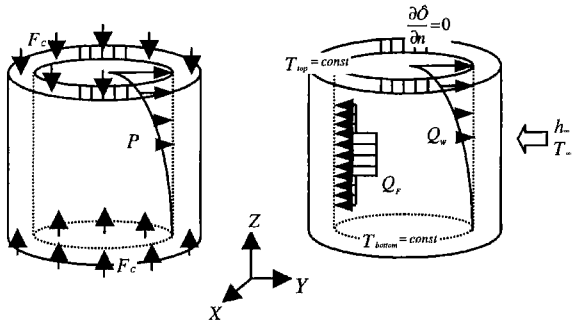

Figure 1. Schematic diagram of geometry and imposed boundary conditions.

coefficient was assumed to be 0.1.

2.2. Boundary Conditions

The cylinder was modeled with specified top and bottom temperatures to simulate cooling effects, and the part of the top beneath two-quartz window was assumed as an adiabatic zone (see Figure 1, two hatching area on the top) based on material properties of quartz. On the inside cylinder, heat input from the combustion gas, heat generation by piston ring friction, and combustion pressure were applied. On the outside cylinder, cooling by natural and forced convection, and atmosphere pressure were applied.

2.2.1. Heat Flux from Combustion Gas to Cylinder Wall, Q_w

During firing heat loss through head, block and piston is about 25-30% of $\dot{m}_f Q_{LHV}$ and about 30% of previous value (9-10 % $\dot{m}_f Q_{LHV}$) is gone through cylinder liner for the case of conventional engines. In this work, Q_w was assumed 3% of $\dot{m}_f Q_{LHV}$ ($\dot{m}_f$ is 1.13 kg/h and Q_{LHV} is 44 MJ/kg), based on material properties – low thermal conductivity and thermal diffusivity. For motoring, the total heat transfer input from the gas was assumed 6% of $\oint_{cycle} pdv$ during the closed cycle and profile was exactly same as firing case. Figure 2 shows normalized heat fluxes into cylinder wall and suggested profile of previous GM research. The absolute magnitude of these two cases is different because of engine type and operating condition, but profile was much similar.

2.2.2. Frictional Heat Flux to Cylinder Wall, Q_f

During motoring, total friction heat input was calculated by assuming a constant friction coefficient, and integrating the work consumed by friction over a cycle (Syrimis, 1998). Friction power is given by Eq. (1)

$$P_f=\oint_{cycle} (C_f \cdot P_m \cdot A_r \cdot V)dt \quad (1)$$

Total friction power was found to be 190 W, and 33% of this value was assumed to go into the liner. During firing, friction heat input was taken to be 70% of above value, considering piston ring expansion. Normalized profile, based on mean piston speed, is shown in Figure 3.

2.2.3. Heat Transfer Coefficient for Natural Convection

Vertical flat plate correlation was used for the fired and motored operation (Incropera, 1985).

2.2.4. Heat Transfer Coefficient for Moderate Forced Convection and Intensive Forced Convection

Equation around the cylinder shaped object was used for both of the fired and motored operation. (Incropera, 1985). And it was assumed that V_{nozzle} is 1 m/s for moderate cooling and 5 m/s for intensive cooling, respectively.

2.2.5. In-Cylinder Gas Pressure and Clamping Force

Normalized combustion pressure distribution is shown in Figure 4. Since there is no firing data, maximum pressure was assumed to be 6 MPa based on conventional engine data with similar engine geometry. On the top and bottom surface of the model, distributed forces were imposed to simulate clamping forces (see Figure 1).

2.2.6. Mechanical Constraints

As mechanical constraints for stress analysis, selected nodes were located on the top and bottom surfaces were fixed.

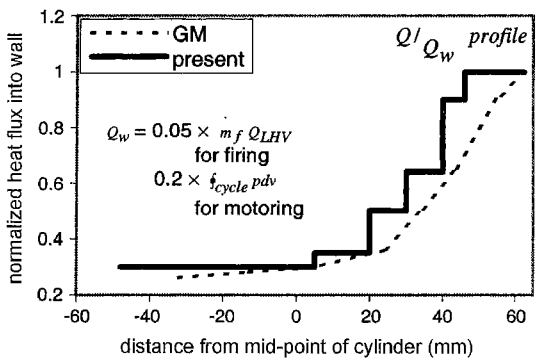

Figure 2. Normalized heat transfer profile compared to the GM suggested profile.

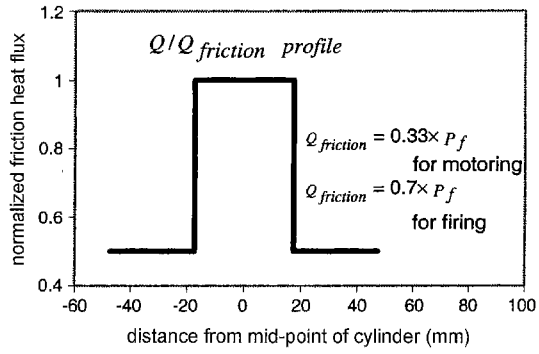

Figure 3. Normalized frictional hat transfer profile.

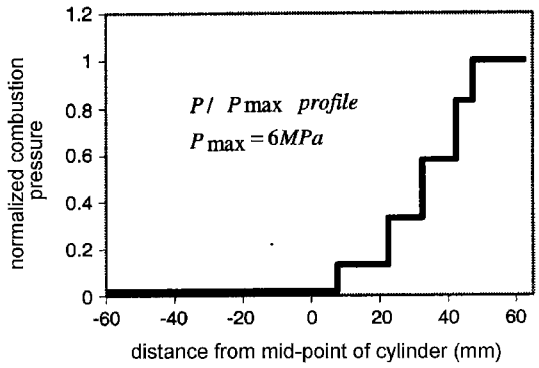

Figure 4. Normalized pressure distribution profile.

3. FEM MODEL VALIDATION

In order to validate thermal boundary condition, model reliability and constraint, outside cylinder temperature was compared to experimental data, and previous study was followed up numerically.

3.1. Experimental Set-up and Method

A single cylinder, optical test engine was used in this study. The primary specifications of the engine are reported in Table 2. Two quartz windows were placed at the top of the quartz cylinder to investigate combustion phenomena.

Three of contact probe type thermocouples were installed at the outside quartz cylinder (5, 55, 82 mm away from the liner top) and external temperatures were recorded from 1200 to 2000 second under the following operating conditions: motored @ 1200 rpm, with and without external forced convection, 30°C (intake air) and 90°C (cylinder head) temperatures, 100 kPa, manifolds absolute pressure, and uncharacterized air jet as external forced cooling.

3.2. Predicted Temperature History and Validation of Thermal Boundary Conditions

To find optimum thermal boundary and to check sensitivity of imposed boundary conditions, a total 9 sets of boundary conditions were examined under motored condition. Each case is shown in Table 3. Measured and predicted transient surface temperature at given location (below 5, 55, 82 mm from liner top) were compared in Figures 5 and 6. As a result, case present was chosen as a reasonable thermal boundary condition set, considering

Table 2. Specification of test engine in mm.

Bore	Stroke	Con. rod	Liner length	Cylinder thickness	Comp. ratio
92	96	223.5	124.8	13.625	9.5

Table 3. Thermal boundary conditions for model validation.

Case	Cyclic heat flux input (%) of $\oint_{cycle} pdv$	Frictional heat flux input (%) of P_f	Outside cooling	
			Natural	Forced
Present	6	33	O	O
1	4	33	O	
2	8	33	O	
3	6	25	O	
4	6	40	O	
5	4	33		O
6	8	33		O
7	6	25		O
8	6	40		O

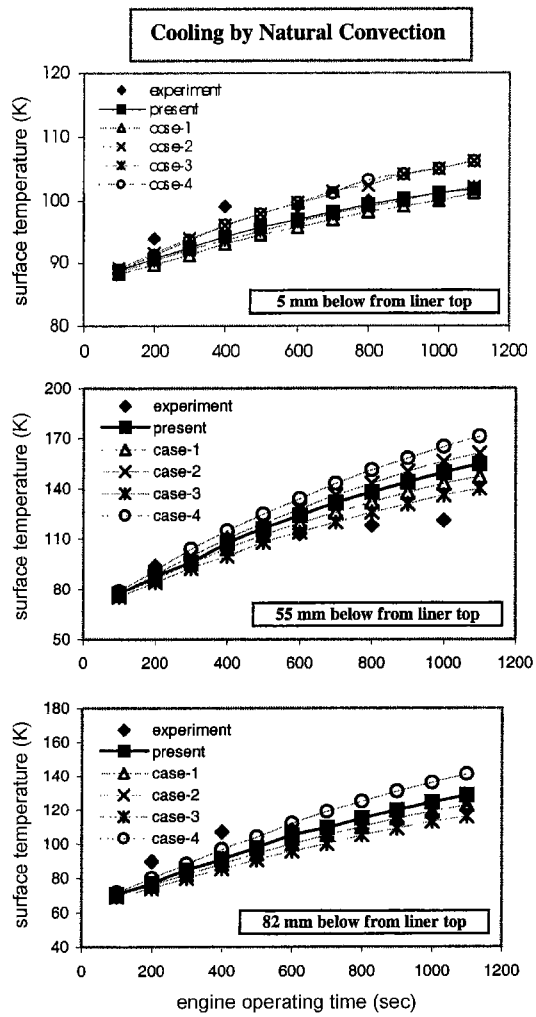

Figure 5. Comparison between measured and predicted transient outside temperature [K] with natural convection during motoring.

results of whole computational domain. Some differences were observed in each case especially before about 1000 second, but trend was is satisfactory. The discrepancies mentioned above can be attributed to the following reasons. First, there is some possibility of maldistribution of cooling air-jet under forced convection. Second, there are many assumptions such as heat flux into inside liner wall, outside temperature and heat transfer coefficient, to impose thermal boundary conditions because of lack of basic data about combustion phenomena in quartz engine.

Comparing these two results, it is concluded that the FEM model and the applied boundary conditions used in this study have the potential to capture the thermal and stress field within the quartz cylinder with acceptable accuracy.

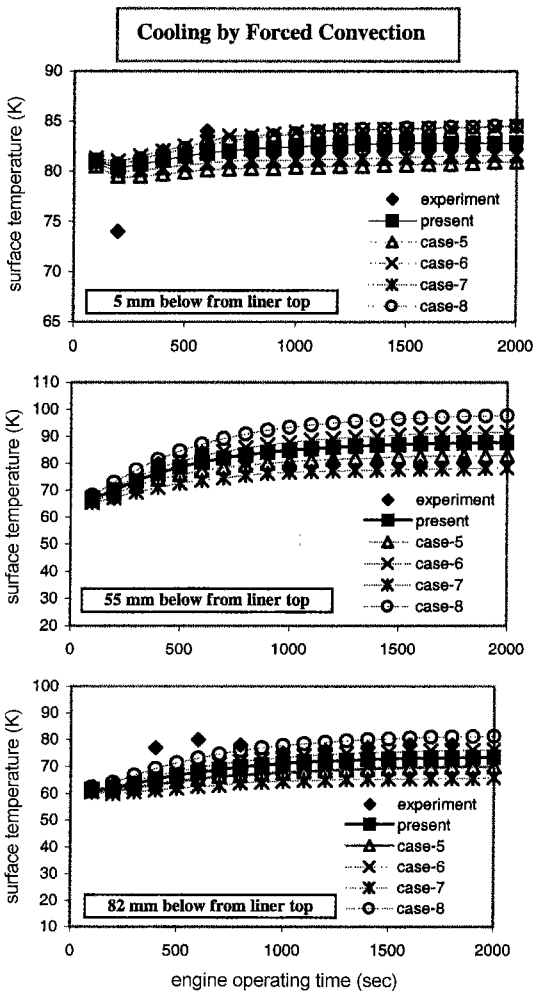

Figure 6. Comparison between measured and predicted transient outside temperature [K] with forced convection during motoring.

4. TEMPERATURE AND STRESS DISTRIBUTION

4.1. Effect of Quartz Window

Two quartz windows were located on the liner top to observe in-cylinder flow field and engine combustion phenomena. Since quartz has low thermal conductivity and low thermal expansion coefficient, the effect of quartz window on temperature and stress field was examined under intensive forced cooling, with ring friction and 2000 psi clamping force. The results are shown in Figures 7 and 8, and boxes with dashed line on the liner top indicate quartz window location. For the case of no window (see Figure 7), evenly distributed hot region was found near the mid-stroke because of combination of combustion and friction heat input. Otherwise, hot region was observed beneath window because heat flux hardly went through the quartz window (see Figure 8). As a result, maximum temperature of case with window was about 100 K higher and distribution shape was very different. On the other hand, maximum normal stress increased little bit (0.9 MPa), but overall distribution shape was very similar. Hence, quartz window effect on maximum stress was negligible.

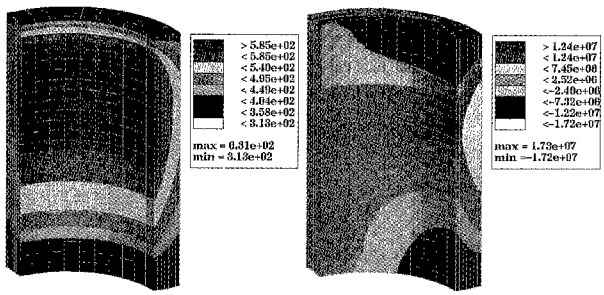

Figure 7. Steady state temperature [K] and maximum normal stress [MPa] distribution without quartz window.

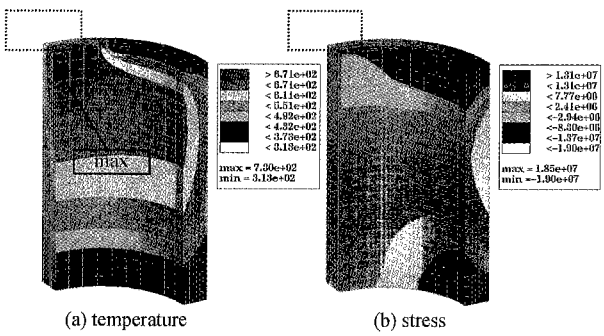

Figure 8. Steady state temperature [K] and maximum normal stress [MPa] distribution with quartz window.

4.2. Effect of Piston Ring Friction

The effect of piston ring friction on temperature and stress field was tested under the following boundary conditions: intensive forced cooling, with quartz window and 2000 psi clamping force. Figure 9 shows temperature and maximum normal stress distribution without frictional heat source. For the case of ring friction (see Figure 8), maximum temperature was found at the relatively lower point than that of case without ring friction. And a few more temperature gradient was found on the cross-section, that is, larger thermal stress can be induced in this case. Maximum temperature of case without ring friction (see Figure 9) was about 40 K lower and distribution shape was different. Maximum normal stress was somewhat smaller, but was found at exactly same point and overall distribution shape was very similar. Therefore, the effect of ring friction on maximum stress level was not serious.

4.3. Effect of Cylinder Material

Sapphire and quartz were examined as the cylinder material under the same boundary conditions (intensive forced cooling, with window, with ring friction, and 2000 psi clamping force) and geometry. These materials are very brittle and ultimate tensile strength is known as 400 MPa for sapphire and 50 MPa for quartz (relatively weaker than sapphire). Figure 10 shows temperature and maximum normal stress distribution of sapphire cylinder. Since thermal conductivity of sapphire is about 18 times larger than quartz, less number of isotherm was existed beneath window and hot region was well distributed than quartz. Because thermal expansion coefficient is about 14 times larger than quartz, it made huge thermal stress and the characteristics of isostress were shown symmetry shape. Predicted maximum normal stress was 578 MPa (safety factor=0.7) and 18.5 MPa (safety factor=2.7) for sapphire and quartz, respectively. As a result, maximum temperature of sapphire cylinder was about 320 K lower and maximum normal stress was about 30 times larger than quartz. And the overall shape of temperature and

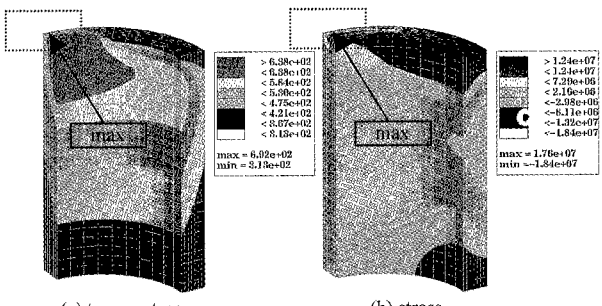

Figure 9. Steady state temperature [K] and maximum normal stress [MPa] distribution without ring friction.

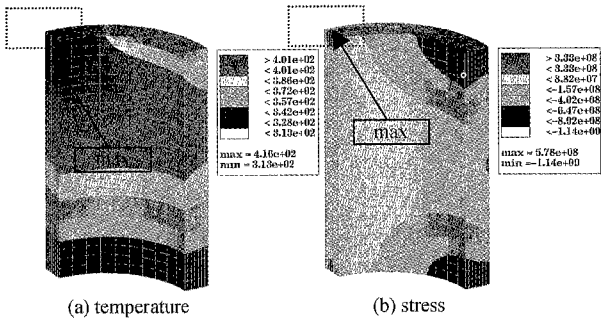

Figure 10. Steady state temperature [K] and maximum normal stress [MPa] distribution of sapphire cylinder.

stress distribution was fairly different. Therefore, quartz was suitable material for the cylinder under given conditions in this study.

4.4. Effect of Forced Convection

The effects of natural convection, moderate forced convection and intensive forced convection were examined under the following conditions: with window, with ring friction and 2000 psi clamping force in order to validate effectiveness of forced convection. Maximum transient temperature and maximum normal stress are shown in Figure 11, and temperature and maximum normal stress distribution are shown in Figures 12 and 13. In Figure 11, three different slopes were observed, depending on effects of temperature gradient and mean body temperature. It shows the steepest slope trend between 0 and about 100 second, and the 2nd steepest between from 100 to about 1200 second. After then, under forced convection, these trends seem to close to the steady state asymptotically. In case of natural convection, however, the slope still increased, that is, it needs more time to approach to the steady state. These trends mentioned above can be explained that: (1) Since the effect of thermal penetration into quartz liner, which has room temperature initially, caused large temperature gradient, temperature gradient was more dominant than mean body temperature before about 1000 second. (2) Once quartz liner was heated up (after about 1000 second), the effect of mean body temperature on thermal stress and material safety was more dominant. Maximum temperature was almost same until 100 second because thermal penetration time ($\tau \cong \delta^2/\alpha$) is about 232 second for this engine, that is, external cooling was not much effective until it passed over thermal penetration time. Transient temperature distribution of quartz cylinder under intensive forced convection is shown in Figure 12. Before 1000 second, hot region was found near the liner top, and maximum temperature was observed beneath quartz window because heat flux could not go through the quartz window and

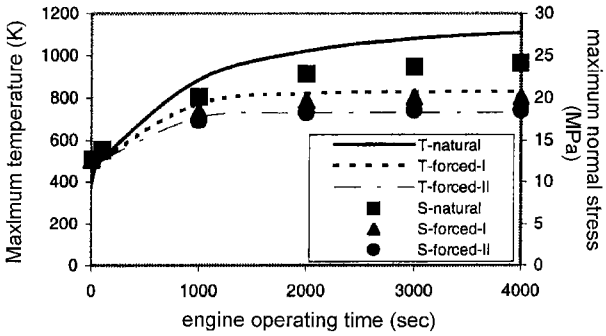

Figure 11. Transient maximum temperature [K] and maximum normal stress [MPa].

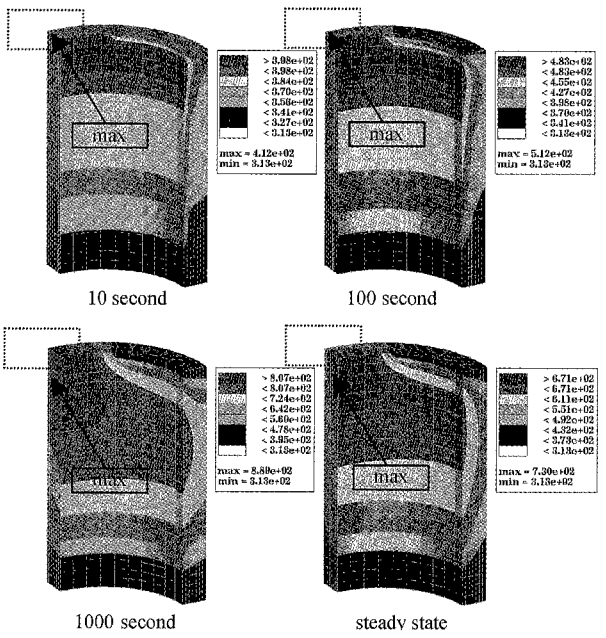

Figure 12. Transient temperature distribution [K].

frictional heat input was not much yet. During this period, it seems that the effect of outside cooling was not effective. After 1000 second, the hot region was prevailed toward mid-stroke and maximum temperature was found at about 10 mm lower point than that of the early combustion stage because of piston ring friction. In general, the region with large temperature gradient was observed beneath quartz window and on longitudinal cross-section.

Figure 13 shows transient maximum normal stress distribution of quartz under intensive forced convection. Overall distribution shape of each case was similar and higher stress concentration region was found in the same region with higher temperature and lager temperature

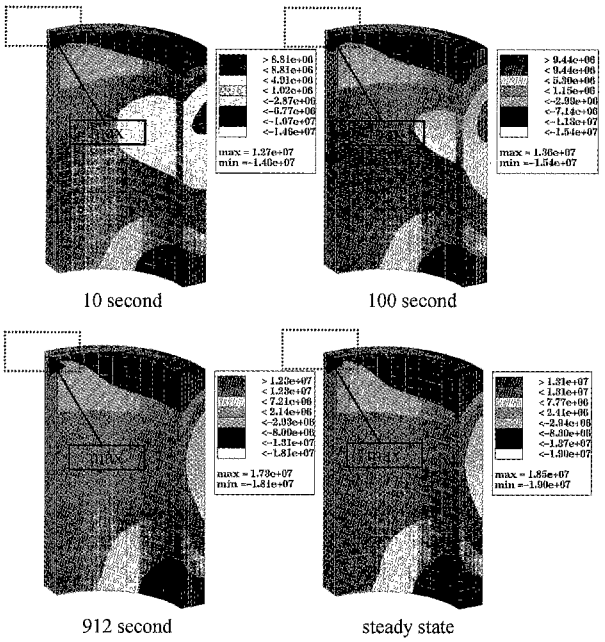

Figure 13. Transient maximum normal stress distribution [MPa].

gradient (see Figure 12). It is important to compare the stress results to temperature distribution. Thermal stress is mainly induced from temperature gradient and mean body temperature (Spalding, 1989). Maximum normal stress was found beneath quartz window in every case and at every time step under given conditions.

Maximum temperature was 1100 K in natural convection, 830 K in moderate forced convection and 730 K in intensive forced convection, respectively. At the steady state, the maximum normal stress in natural convection was reached about 130% (24.1 MPa) of that of intensive cooling case and the moderate cooling case was reached about 110% (20.1 MPa). Therefore, forced convection of the outside cylinder was very helpful to decrease maximum stress level.

4.5. Effect of Clamping Force

Three kinds of clamping forces (1000, 2000 and 3000 psi) based on the practical value 2000 psi were imposed on the top and bottom surfaces to investigate the clamping force effect on maximum normal stress under the following conditions: intensive forced cooling, with window and with ring friction. Overall distribution shape of temperature and stress was fairly similar to general case. The maximum normal stresses were 18.0, 18.5 and 19.0 MPa for 1000, 2000 and 3000 psi, respectively. Increasing clamping force made peak stress increase but it does not make any serious effect on failure between 1000 and 3000 psi (safety factor=2.6-2.7) under given

Table 4. Summary of relative importance between thermal load and combustion pressure effects on maximum normal stress [MPa].

Material	Thermal load	Combustion pressure	Total
Sapphire	572	6.95	578
Quartz	12.4	7.12	18.5

conditions.

4.6. Effect of Thermal Load and Combustion Pressure

To investigate the relative importance between thermal load and combustion pressure, models made of sapphire and quartz were examined under the following conditions: intensive forced cooling, with window, with ring friction and 2000 psi clamping force. Coupled total stress can be calculated by ($\sigma_{thermal}+\sigma_{mechanical}$) and the results of maximum normal stress are summarized in Table 4. The effect of thermal load was the most dominant factor for sapphire. For the quartz cylinder, however, the relative magnitude of stress due to combustion pressure was about 57% of pure thermal stress. Hence, both kinds of stresses should be considered deliberately.

4.7. Effect of Cylinder Thickness

The cylinder thickness was changed to find optimum cylinder thickness under the following conditions: intensive forced cooling, with window, with ring friction and 2000 psi clamping force. Maximum normal stress results are shown in Figure 14. Regarding stress due to combustion pressure, the thicker the thickness of cylinder was, the smaller the stress level became because of reinforcement effect. Maximum temperature did not increased above model thickness of 13.625 mm, but the stress due to pure thermal load increased continuously. As mentioned foregoing section, a thermal stress is induced mainly from two reasons – temperature gradient and mean body temperature. Although there was no maximum temperature change, model thickness was still increasing. Consequently, large temperature gradient was induced, that is, thermally induced stress had kept increasing. According to these results, thermal stress was more dominant effect on maximum normal stress. Therefore, from the material cost and safety point of view, optimum thickness would be around between 13 and 14 mm.

4.8. Failure Prediction

To predict engine component failure during the operation is one of the most important procedures for developing new engines. The maximum normal stress theory agrees with test data for brittle materials and is generally

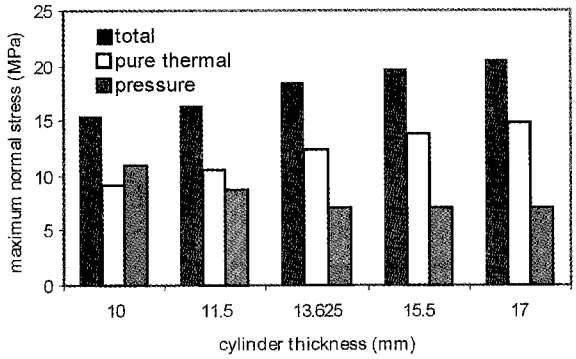

Figure 14. Effect on cylinder thickness on maximum normal stress [MPa].

accepted in design practice for such materials (Higdon, 1985). The maximum normal stress predicts failure of a specimen subjected to any combination of loads when the maximum normal stress at any point reaches the axial failure stress as determined by an axial tensile or compressive test of same material. Sapphire and quartz are extremely brittle materials and the maximum normal stress theory was used to predict quartz failure. Until now, the followings have been known as main reasons for quartz engine failure: (1) thermal stress (2) accumulating large chips from mounting errors and small chips from assembly error. Allowable temperature of quartz for continuous operation and ultimate tensile strength are known as 1200 K and 50 MPa, respectively. In natural convection case, the maximum normal stress was 24.1 MPa and it was satisfactory with a safety factor of about 2.0. But the maximum temperature was 1110 K and it seems not safe. On the other hand, quartz cylinder with 13.625 mm thick under the intensive forced convection can be operated with a safety factor of about 2.7 without any concern about temperature limit under any given clamping force.

5. CONCLUSION

There has been no indication from the experimental and analytical results, which is capable of causing a sudden quartz cylinder breaking. This work has conducted the important issue of developing a quartz cylinder. It has given us good qualitative and quantitative results of temperature and stress fields in the quartz cylinder. The following conclusions drawn from this study can be useful for improving current quartz engine technique:

Forced convection of outside cylinder is very effective method to decrease the maximum stress level. In natural convection case, engine can be operated with a safety factor of about 2.0. However, the maximum temperature was near allowable continuous operation limit of quartz.

On the other hand, quartz cylinder under intensive forced convection can be operated with a safety factor of about 2.7 and without concern about the maximum temperature limit.

The effect of thermal load is the most dominant factor for sapphire cylinder. On the other hand, since the relative magnitude of stress due to combustion pressure was about 57% of pure thermal stress, both kinds of stresses should be considered deliberately for quartz cylinder.

Increasing clamping forces make maximum stress level increase. However, it does not make any serious effect on failure between 1000 and 3000 psi. And optimum thickness would be around between 13 and 14 mm from the material cost and safety point of view.

ACKNOWLEDGEMENT–The authors gratefully acknowledge financial support by fellowship from Korea Science and Engineering Foundation.

NOMENCLATURE

Ar	ring contact area
C	constant
C_f	friction coefficient
D	hydraulic diameter
F_c	clamping force
G_L	grashof number
$\bar{h}$	convection heat transfer coefficient
h_∞	ambient convection heat transfer coefficient
k	thermal conductivity
L	length
$\dot{m}_f$	fuel mass flow rate
n	constant or arbitrary direction
Nu	nusselt number
P	pressure
p_f	frictional power
p_m	motoring pressure
P_{max}	peak pressure
Pr	prandtl number
Q	heat flux
Q_f	heat flux due to ring friction
$Q_{friction}$	heat flux due to ring friction
Q_{LHV}	low heating value of fuel
Q_w	heat flux from combustion gas to inside wall
Ra	rayleigh number
Re	reynolds number
S-	indicates stress
T-	indicates temperature
T_s	film temperature
T_{top}	liner top temperature
T_{bottom}	liner bottom temperature
T_∞	ambient temperature
V	instantaneous piston speed
V_{NOZZLE}	nozzle exit velocity
α	thermal diffusivity
β	thermal expansion coefficient
δ	thermal penetration depth
ν	dynamic viscosity
τ	thermal penetration time

REFERENCES

Bates, S. C. (1988). A Transparent Engine for Flow and Combustion Visualization Studies, *SAE* 880520.

Bowditch, F. W. (1961). A New Tool for Combustion Research A Quartz Piston Engine, *SAE Transaction.* **69**, 17-23.

Grosser, M. (1978). Diesel, *The Man and the Engine*, Atheneum.

Higdon, A., Ohlsen, E. A., Stiles, W. B., Weese, J. A., and Riley, W. F. (1985). *Mechanics of Materials*, 4th edn. John Wiley & Sons.

Holtman, R. L. and McClure, P. B. (1978). Detroit Diesel Allison, Indianapolis. Indiana. private communication.

Incropera, F. P. and DeWitt, D. P. (1985). *Introduction to Heat Transfer*, 2nd edn. John Wiley & Sons.

Ishikawa, N. and Daily, J. W. (1978). Observation of Flow Characteristics in a Model I.C. Engine Cylinder, *SAE* 780230.

Nakanishi, K., Hirano, T., Inoue, T., and Ohigashi, S. (1975). The Effect of Charge Dilution on Combustion and Its Improvement Flame Photograph Study, *SAE* 750054.

Namazian, M., Hansen, S., Lyford-Pike, E., Sanchez-Barsse, J., Heywood, J. B., and Rife, J. (1980). Schlieren Visualization of the Flow and Density Fields in the Cylinder of a Spark-Ignition Engines, *SAE* 800044.

Oppenheim, A. K., Cheng, R. K., Teiehman, K., Smith, O. I., Sawyer, R. F., Hom, K., and Stewart, H. E. (1976). A Cinematographic Study of Combustion in an Enclosure Fitted with a Reciprocating Piston, *Conference on Stratified Charge Engines*, London. England.

Richman, R. M. and Reynolds, W. C. (1984). The Development of a Transparent Cylinder Engine for Piston Engine Fluid Mechanics Research, *SAE* 84037.

Spalding, D. B. and Afgan, N. H. (1989). *Heat & Mass Transfer in Gasoline and Diesel Engines*, Hemisphere Publishing Co..

Syrimis, M. and Assanis, D. (1998). Thermal Modeling of the GM Quartz Engine, project report.

Withrow, L. and Rassweiler, G. M. (1936). Slow-Motion Shows Knocking and Non-Knocking Explosions, *SAE Transaction.* **39**, 297-303.